Journal of Materials Chemistry B

ROYAL SOCIETY OF CHEMISTRY

PAPER

View Article Online
View Journal | View Issue

Cite this: *J. Mater. Chem. B*, 2021, **9**, 2666

Synthesis, molecular docking calculation, fluorescence and bioimaging of mitochondria-targeted ratiometric fluorescent probes for sensing hypochlorite *in vivo*†

Ling Huang, Wanting Su, Yuping Zhao, Jingting Zhan and Weiying Lin *

Received 23rd November 2020,
Accepted 3rd February 2021

DOI: 10.1039/d0tb02735a

rsc.li/materials-b

Mitochondria are the main sites for the production of hypochlorite (OCl^-). The protein adenine nucleotide translocase (ANT) is located in the inner mitochondria membrane, which is mainly participated in the transportation of ions and metabolites. At the cellular organelle level, overexpression of ANT is associated with enhanced production of OCl^-, however, abnormal levels of OCl^- cause redox imbalance and loss of function of mitochondria. Herein, a novel mitochondria-targeted ratiometric fluorescent probe **Mi-OCl-RP** has been developed. Molecular docking calculation suggested a potential molecular target for the probe in the ANT, and the high binding energy (−8.58 kcal mol^{-1}) may explain the high mitochondria selectivity of **Mi-OCl-RP**. The unique probe exhibits excellent spectral properties including ratiometric fluorescence response signals to OCl^- (within 7 s), high selectivity and sensitivity, and a large Stokes shift (278 nm). In addition, the colocalization coefficient confirms that **Mi-OCl-RP** can effectively target mitochondria. Furthermore, **Mi-OCl-RP** has low toxicity and good permeability, and was successfully employed in ratiometric imaging of OCl^- *in vivo*, affording a robust molecular tool for investigating the biological functions of OCl^- in living systems.

Introduction

Mitochondria, as one of the most important subcellular organelles, are involved in a variety of key cellular processes, including the production of reactive oxygen species (ROS), regulation of programmed cell death, and maintenance of cellular protein homeostasis.[1,2] The protein adenine nucleotide translocase (ANT) is among the most abundant proteins in the inner mitochondria membrane, which is mainly participated in the transportation of ions and metabolites through the mitochondria inner membrane.[3,4]

Overexpression of ANT is associated with enhanced production of ROS, which mediates cell death *via* ROS-dependent upregulation.[5] ROS are a family of molecular oxygen derivatives and free radicals with redox activity, which are produced in a kind of physiological process.[6–9] Hypochlorite (OCl^-) is a vital member of ROS and plays a crucial role in a range of physiological and pathological processes in the human body, such as antibacterial and anti-inflammatory physiological defence functions.[10–13] Nevertheless, abnormal levels of OCl^- have been implicated in a variety of diseases, including cardiovascular diseases, neurodegenerative conditions, arthritis, and cancer.[14–19]

Additionally, the active mitochondria of mammals are the main part of ROS production, with a pH range of weak alkaline (~8.0), and are vulnerable to ROS attack and damage, resulting in mitochondria dysfunction.[20–22] Compared with other analytical methods, fluorescence imaging is one of the most favorable techniques to detect biological molecules and biological parameters in living systems because of its high sensitivity and selectivity, non-interference detection, real-time imaging, convenient sample preparation and spatial resolution. So far, some fluorescent probes for the detection of OCl^- in mitochondria have been made.[23–26] However, most of the reported probes exhibit relatively short Stokes shifts, and the potential mitochondria-targeted protein obtained by molecular docking calculations is not studied (Table S1, ESI†). Therefore, it is critical to study potential mitochondria-targeted proteins by molecular docking calculations and development of a ratiometric fluorescent probe with a large Stokes shift for response to OCl^- in mitochondria.

In this paper, a new ratiometric fluorescent probe **Mi-OCl-RP** is constructed based on the mechanism of internal charge transfer (ICT) processes. Molecular docking calculations are used to identify possible binding sites of **Mi-OCl-RP** in mitochondria against a potential molecular target, that is, ANT.

Guangxi Key Laboratory of Electrochemical Energy Materials, Institute of Optical Materials and Chemical Biology, School of Chemistry and Chemical Engineering, Guangxi University, Nanning, Guangxi 530004, P. R. China.
E-mail: weiyinglin2013@163.com

† Electronic supplementary information (ESI) available: Supplementary spectra, NMR and HRMS data. See DOI: 10.1039/d0tb02735a

The molecular docking mode shows high affinity of the probe to ANT in mitochondria, providing high feasibility for the specific targeting ability of the probe in mitochondria. The probe recognizes OCl^- with an ultrafast response, a large Stokes shift, and high selectivity and sensitivity. In addition, the colocalization coefficient supports that **Mi-OCl-RP** can effectively target mitochondria. Finally, the imaging experiments of living cells and zebrafish confirm that **Mi-OCl-RP** can be used to monitor the level of OCl^- *in vivo*.

Experimental section

Molecular docking calculations

Atomic coordinates for ANT were obtained from the crystallographic structure solved at the RCSB Protein Data Bank. Molecular docking simulations were performed with the program AutoDock 4.2. The ligands were first optimized for an optimal structure with chembio3D Ultra 14.0. The rigid conformation docking between the dehydrogenated ANT and the probe was carried out. The grid maps were calculated by using AutoGrid. The Lamarckian genetic algorithm was adopted in this work. Other parameters set to default. The binding energy was obtained for further analysis.

Spectral measurements

The stock solution of 1 mM probe was fresh in dry methanol and stored at 4 °C. The various testing analyte stock solutions were prepared at 10 mM in twice distilled water. The test solution contained the probe and an analyte, and was tested in pH 7.4 PBS buffer (20 mM, 1% methanol). Then, the absorption and fluorescence spectra were recorded.

Imaging of exogenous and endogenous OCl^- in living cells

Human lung cancer cell line (A549 cells), human breast cancer cell line (MCF-7 cells), and macrophage (RAW264.7) were seeded into 35 mm glass-bottom culture dishes and cultured for 24 h. For the imaging of exogenous OCl^-, A549 and MCF-7 cells were pre-treated with OCl^- (5, 8 and 10 μM) for 10 min, and then incubated with **Mi-OCl-RP** (10 μM) for 20 min at 37 °C in the incubator. For the imaging of endogenous OCl^-, RAW264.7 cells were divided into four groups. In one group, the cells were treated with **Mi-OCl-RP** (10 μM) for 20 min at 37 °C in the incubator. Another two groups, LPS (1.0 μg mL^{-1}) for 3 h or ABAH (200.0 μM) for 1 h were incubated with 10.0 μM **Mi-OCl-RP** in culture media for another 20 min at 37 °C. The last group, LPS (1.0 μg mL^{-1}) for 3 h and then ABAH (200.0 μM) for 1 h were incubated with 10.0 μM **Mi-OCl-RP**. Before imaging, the cells were washed three times with PBS buffer. The A549 cells, MCF-7 cells and RAW264.7 cells were tested under excitation at 405 and 588 nm, respectively.

Colocalization experiment

For confirming the intracellular localization of the probe, A549 cells were used to colocalize the probe and Mito Tracker Green. The cells were treated with **Mi-OCl-RP** (10 μM) for further incubation for 15 min at 37 °C in the incubator and then treated with 100 nM Mito Tracker Green for another 5 min. Then the cells were washed with PBS prior to imaging. The A549 cells under excitation were tested at 405, 490 and 588 nm, respectively.

Imaging of OCl^- in zebrafish

Zebrafish were purchased from Nanjing Eze-Rinka Biotechnology Co., Ltd. All animal experiments were carried out in compliance with the guidelines for the requirements of Laboratory Animals of Guangxi University. One group of zebrafish was incubated with **Mi-OCl-RP** (10 μM) stock solution at room temperature for 30 min. Under the same condition, the other groups were pre-treated with different concentrations of OCl^- (5, 8, and 10 μM) for 10 min, and then 10 μM of **Mi-OCl-RP** was added for another 30 min. Then, the four groups were transferred to the new glass chassis for imaging. The zebrafish were imaged by a 4 × objective lens confocal microscope.

Result and discussion

Design and synthesis of mitochondria-targeted ratiometric fluorescence probe Mi-OCl-RP

Cyanine is an important fluorescent dye with prominent spectral properties such as high fluorescence quantum yield and molar absorption coefficient, which is used as a desirable fluorescent platform for research and application extensively.[27,28] Moreover, phenyl isothiocyanate is an electron-donating group, and could be easily oxidized by OCl^- to provide sulfoxide atoms with electron-donating properties.[29–31] Thus, we selected cyanine dye as the fluorescent emitter, and sulfur atoms of the phenyl isothiocyanate group as a specific recognition group for OCl^- based on the fluorescence mechanism of intramolecular charge transfer (ICT) to design the probe **Mi-OCl-RP** (Scheme 1). The cyanine moiety was used to provide absorption and emission.

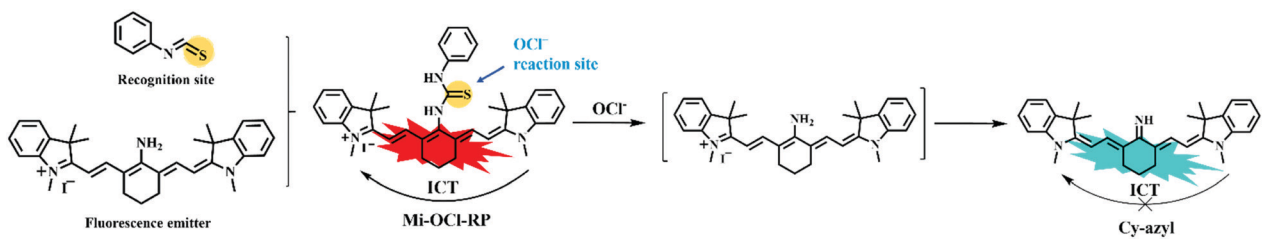

Scheme 1 Rational design of the probe **Mi-OCl-RP** reporting OCl^-.

Table 1 Binding energy of **Mi-OCl-RP** and ANT

Conformation	Affinity (kcal mol^{-1})	Conformation	Affinity (kcal mol^{-1})
1	−8.58	6	−7.51
2	−8.28	7	−7.42
3	−8.01	8	−6.96
4	−7.66	9	−6.69
5	−7.51	10	−6.13

It is expected that nucleophilic substitution of the phenyl isothiocyanate group by OCl^- would release a cyanine unit of secondary amines, which undergoes primary–secondary amine tautomerization to form **Cy-azyl**. This tautomerization would shift emission and absorption distinctly, showing ratiometric fluorescence and photoacoustic response to OCl^-. The probe was prepared *via* reaction of the corresponding phenyl isothiocyanate group with cyanine. The details of the synthetic procedure of the probe are described in the ESI.† The chemical structures are verified by ^{1}H NMR, ^{13}C NMR and HRMS analysis.

ANT in mitochondria may be a suitable candidate that serves as a molecular target.[32,33] Potential interactions of **Mi-OCl-RP** and ANT are investigated by molecular docking calculations. Table 1 shows the binding energy of interaction between **Mi-OCl-RP** and ANT in the various conformations. The binding sites and interactions are shown in Fig. 1 and Fig. S1 (ESI†), and the various conformations are held in an active pocket of ANT by forming intermolecular forces (π–π, π–cation, hydrophobic and van der Waals' interactions). The binding energy of conformation **1** reaches −8.58 kcal mol^{-1}, which may be caused by π–π interactions between the phenyl moiety of the positively charged cyanine structure and the amino acid PHE81 (Fig. 1). The bonding processes of conformations **2** and **3** have also π–cation or π–π interaction. Compared with the binding energy of conformation **1**, the affinity energies of conformations **2** and **3** are also up to −8.28 and −8.01 kcal mol^{-1}, with the potential result of the interaction between the phenyl moiety of the isothiocyanate group and the amino acid residues (LYS271 and TRP70, respectively) (Fig. S1 **2a** and **3a**, ESI†). Similarly, conformation **9** has π–π interactions. Nevertheless, the affinity energy of conformation **9** is only −6.69 kcal mol^{-1}. This may be due to the phenyl moiety of the non-positively charged cyanine structure and the amino acid PHE271 interaction (Fig. S1 **9a**, ESI†). The results show that the π–π bonds may play a significant role in the high binding energy (−8.58 kcal mol^{-1}) between **Mi-OCl-RP** and ANT.

In this binding model, the intermolecular forces played a major role in the interaction between **Mi-OCl-RP** and the amino acid residues of ANT. The results suggest that strong intermolecular forces promote **Mi-OCl-RP** targeting to mitochondria, and the high binding energy (−8.58 kcal mol^{-1}) may explain the high mitochondria selectivity of **Mi-OCl-RP**. Thus, we hypothesize that as a molecular target of **Mi-OCl-RP**, ANT may translocate it into the mitochondria by intermolecular forces.

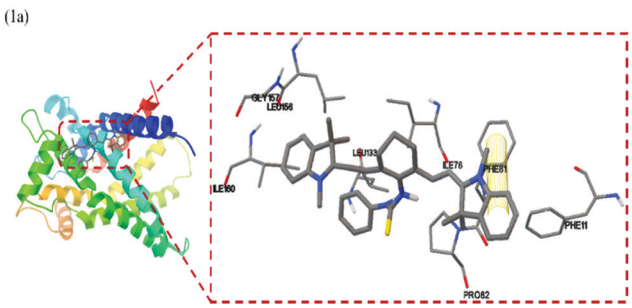

Fig. 1 Molecular binding modeling of conformation **1**. Tertiary structure of ANT, active site and residues of (**1a**) ANT (PDB: 1OKC). The π–π interaction is indicated by a golden block.

Spectral properties of Mi-OCl-RP

The UV-vis absorption response of **Mi-OCl-RP** to OCl^- was examined in pH 7.4 PBS buffer (20 mM, 1% methanol), which exhibited similar changes after reaction with OCl^-. NaOCl was selected as a OCl^- source. As shown in Fig. 2a, the absorption spectrum of **Mi-OCl-RP** (10 μM) showed a strong absorption band at 580 nm and a middle band at 380 nm. After reaction with OCl^- (0–10 μM), **Mi-OCl-RP** not only showed an absorption band with the peak at 580 nm reduced, but a new band centered at 380 nm increased prominently with an isosbestic point at 440 nm, which could be attributed to the formation of **Cy-azyl**.

The emission spectrum of **Mi-OCl-RP** exhibited a main emission band centered at 651 nm and a minor broad band

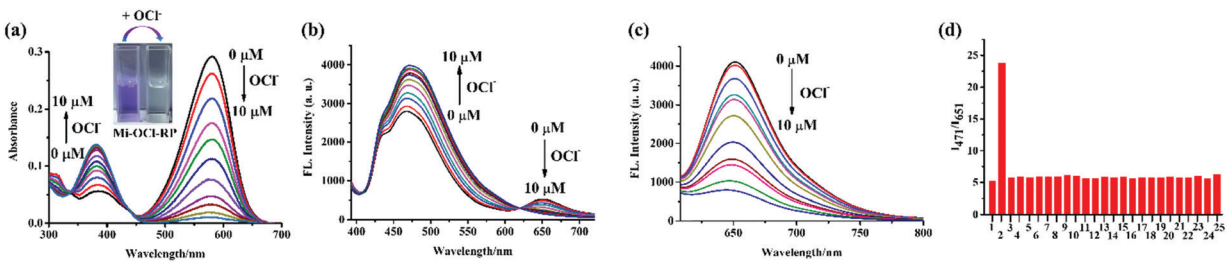

Fig. 2 (a) UV-vis absorption and (b and c) fluorescence spectra of **Mi-OCl-RP** (10 μM) in the presence of 0–10 μM OCl^- in pH 7.4 PBS (20 mM, 1% MeOH). ((b): λ_{ex} = 373 nm; (c): λ_{ex} = 588 nm.) (d) Ratios of fluorescence intensity (I_{471}/I_{651}) of the probe (10 μM) to various relevant species (10 μM): (1) blank; (2) OCl^-; (3) hydroxyl radicals; (4) Cys; (5) Hcy; (6) glutathione; (7) CH_3COOOH; (8) H_2O_2; (9) *t*-butylhydroperoxide; (10) NO; (11) Ca^{2+}; (12) Zn^{2+}; (13) Co^{2+}; (14) Cu^{2+}; (15) Fe^{2+}; (16) Mg^{2+}; (17) F^-; (18) Cl^-; (19) Br^-; (20) I^-; (21) HCO_3^-; (22) SO_3^{2-}; (23) HSO_3^-; (24) NO_2^-; and (25) $ONOO^-$ in pH 7.4 PBS buffer. Inset: Photographs showing the color of 10 μM **Mi-OCl-RP** before and after the addition of OCl^- (10 μM) to the solution. ((d): λ_{ex} = 373 nm.).

centered at 471 nm (λ_{ex} = 373 nm), as shown in Fig. 2b. Meanwhile, under excitation at 588 nm, it showed a strong emission band at 651 nm (Fig. 2c). Therefore, the Stokes shift value is calculated to be 278 nm (under excitation at 373 nm, the emission band of **Mi-OCl-RP** is concentrated at 651 nm). With the concentration increase of OCl^-, the strong fluorescence intensity of **Mi-OCl-RP** at 471 nm increased and an emission band at 651 nm decreased, the color of the solution changes from violet-blue to light yellow and could be detected even by the naked eyes. These results allow for ratiometric (I_{471}/I_{651}) detection of OCl^-. A linear correlation (R^2 = 0.99055) between the emission intensity ratios (I_{471}/I_{651}) and concentration of OCl^- was found in the range of 0–10 μM (Fig. S2a, ESI†). The detection limit was calculated to be 0.35 μM (according to $3\sigma/k$, where σ is the standard deviation of 11 blank measurements, and k is the slope of the linear equation).

To verify the selectivity of **Mi-OCl-RP** for OCl^-, the specificity of **Mi-OCl-RP** was tested in the presence of various relevant analytes. As shown in Fig. 2d, a large ratiometric signal (I_{471}/I_{651}) of 24.5 was observed with **Mi-OCl-RP** in the presence of 10 equiv. of ClO^-. By contrast, with some common anions, including other biological amino acids, ROS and RNS, the ratiometric signal is minimal. Fluorescence intensity of **Mi-OCl-RP** in the presence of OCl^- is much weaker than other analytes under the excitation at 588 nm (Fig. S3b, ESI†). The results show that **Mi-OCl-RP** has excellent selectivity for OCl^-. Then to test the photostability, **Mi-OCl-RP** was irradiated for 40 minutes in the absence and presence of OCl^-, and there was no significant change at 471 and 651 nm (λ_{ex} = 373 and 588 nm) (Fig. S4 and S5, ESI†), indicating that **Mi-OCl-RP** has good anti-photobleaching ability.

As shown in the ESI,† Video S1, it only takes less than 7 seconds to complete the reaction, suggesting that **Mi-OCl-RP** can be used for the real-time ultrafast monitoring of OCl^-. Finally, the pH effect of **Mi-OCl-RP** on the fluorescence properties of OCl^- in the pH range of 4.0–9.0 was also investigated (λ_{ex} = 373 and 588 nm). The fluorescence ratiometric I_{471}/I_{651} at pH 4.0–7.0 remained stable, and increased at pH 7.0–9.0, when OCl^- was added, reaching the highest at pH 8.0 (Fig. S6a, ESI†). Similarly, **Mi-OCl-RP** in the absence and presence of OCl^- (10 μM) at pH 4.0–9.0 showed fluorescence intensity signal under excitation at 588 nm (Fig. S6b, ESI†). These data reveal that **Mi-OCl-RP** could be employed to detect OCl^- under neutral and alkaline conditions.

The energy changes of the Mi-OCl-RP response to OCl^- according to DFT

Density functional theory (DFT) quantum chemical calculation on **Mi-OCl-RP** and its OCl^- adduct was carried out. The energies of the lowest unoccupied molecular orbital (LUMO), the highest occupied molecular orbital (HOMO) and the band gaps (HOMO–LUMO gaps) are shown in Fig. 3. It has been found that the band gap energies of **Mi-OCl-RP** have two values (2.554 eV and 1.127 eV, respectively), which showed two charge transfer characters. The results indicate that **Mi-OCl-RP** exhibits two excited states, which are the same as the UV-Vis absorption spectrum. **Mi-OCl-RP** possessed one electron-withdrawing group (a positive nitrogen moiety of the cyanine group) and two electron-donating groups (no positive nitrogen moiety of the cyanine group and the –NH– moiety), featuring a "push–pull" system to block the ICT process, which led to fluorescence.[34] The ICT process also contributed to the lighting behavior. HOMO, HOMO+1 and LUMO in **Mi-OCl-RP** were located on the fluorophore, the –NH– moiety, and the whole molecular, respectively. The highest-energy transition of **Mi-OCl-RP** came from the HOMO–LUMO and HOMO+1–LUMO orbital transitions. The orbital transition of the HOMO–LUMO (HOMO+1–LUMO) in excited state 1 (excited state 2) indicated a transfer process of one electron from the excited fluorophore unit (the –NH– moiety) to the LUMO of the electron-deficient unit (ICT), leading to fluorescence lighting. However, after the response to OCl^-, the band gap energy of **Mi-OCl-RP** is 3.123 eV, which indicates one charge transfer character (emission state). The results display that **Mi-OCl-RP** has only one emission wavelength, which is similar to the fluorescence spectrum (471 nm).

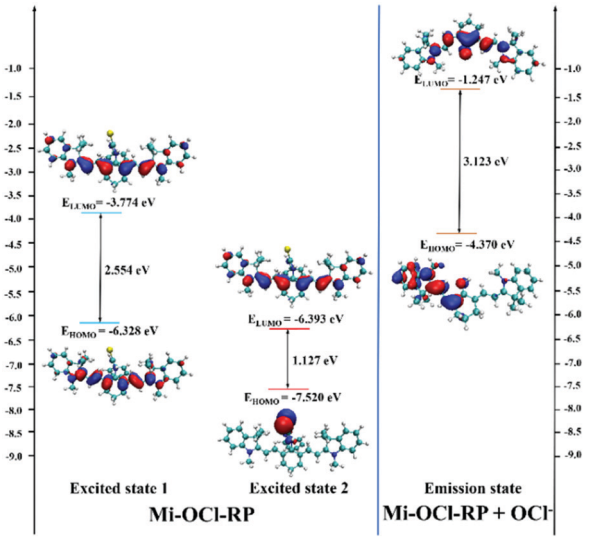

Fig. 3 Theoretical modeling of **Mi-OCl-RP** response to OCl^- calculated by DFT using the optimal structures of the ground and the excited states.

Fluorescence imaging in living cells

Encouraged by the favorable spectral response of the probe to OCl^-, we further assessed the potential application of **Mi-OCl-RP** to detect OCl^- in living cells by dual-color and ratiometric fluorescence imaging. Before that, the cell cytotoxicity of **Mi-OCl-RP** (0–40 μM) to A549 cells, MCF-7 cells and RAW264.7 cells was evaluated by the standard CCK8 assay and the results show that **Mi-OCl-RP** shows a low cytotoxicity to A549 cells, MCF-7 cells and RAW264.7 cells for 24 h (Fig. S7, ESI†), indicating that the probe could be further applied in cell imaging experiments. As shown in Fig. 4 **1a-4b**, the ratio of green and red fluorescence exhibited different fluorescence signals. A549 cells incubated with only **Mi-OCl-RP** (10 μM) showed strong green and red fluorescence signals (Fig. 4 **1b-1c**). However, when the cells were treated with different concentrations of

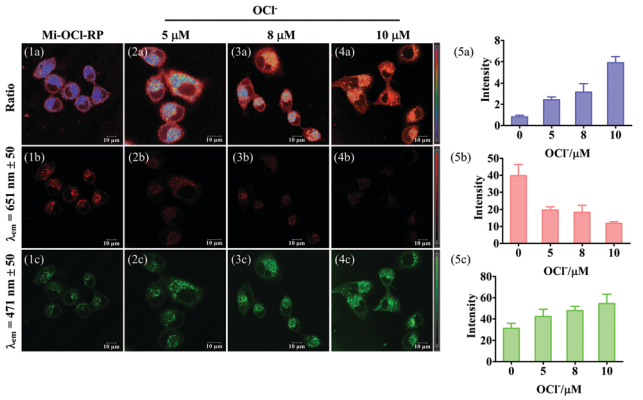

Fig. 4 Confocal fluorescence images of **Mi-OCl-RP** responding to OCl^- in A549 cells. (**1a-1c**) A549 cells incubated with **Mi-OCl-RP** (10 μM, 20 min); (**2a-4c**) A549 cells incubated with OCl^- (5, 8 and 10 μM) for 10 min and then incubated with **Mi-OCl-RP** (10 μM, 20 min). First column: images for the ratios of excitation at 405 and 588 nm; second column: excitation at 588 nm; third column: excitation at 405 nm. (**5a-5c**) Quantified relative fluorescence intensity of images **1a-4c**. Scar bar: 10 μm.

OCl^- (5, 8 and 10 μM), the green fluorescence enhanced as shown in Fig. 4 **2b-4b** and simultaneously the red fluorescence diminished as shown in Fig. 4 **2c-3c**, which is consistent with the results of responding spectra in aqueous solution. We can more intuitively observe the changes in fluorescence signal as shown in Fig. 4 **5a-5c**. At the same time, as shown in Fig. S8 (ESI†), when MCF-7 cells were incubated with the probe and different concentrations of OCl^-, the change of fluorescence intensity was approximately consistent with that of A549 cells. These results illustrate that **Mi-OCl-RP** can be applied for monitoring the level of OCl^- by ratiometric fluorescence imaging in living cells.

Mitochondria are important sites to produce ROS in living cells. The colocalization experiments were performed in A549 cells using **Mi-OCl-RP** and a commercially available Mitochondrial-specific dye (Mito Tracker Green is used to determine the presumed mitochondria-targeted property of the probe). As shown in Fig. 5 **3a-3b**, the fluorescence image of **Mi-OCl-RP** (Fig. 5 **2a-2b**) almost completely overlaps with that of the mitochondria probe (Mito Tracker Green) (Fig. 5 **1a-1b**). Furthermore, the intensity scatter plots and line profiles of **Mi-OCl-RP** and Mito-Tracker Green showed high correlation (Fig. 5 **4a-5b**), indicating that **Mi-OCl-RP** is mainly localized in mitochondria of living cells, and the Pearson's co-localization coefficients were calculated to be 0.87 and 0.86, respectively. The colocalization experiment suggests that **Mi-OCl-RP** targeted mitochondria, which is consistent with the theoretical results of the potential mitochondria-targeted protein obtained by molecular docking calculation. The results establish that **Mi-OCl-RP** is cell membrane permeable and could be used as a fluorescent probe to image OCl^- in mitochondria of living cells.

Ratiometric fluorescence imaging of endogenous OCl^-

To further demonstrate that **Mi-OCl-RP** is used for the detection of endogenous OCl^-, the fluorescence variation of **Mi-OCl-RP** in monocyte-macrophages (RAW264.7) was investigated, considering that this immune cell can be stimulated to produce high levels of intracellular ROS. In order to produce high concentrations of OCl^- in macrophages, the cells were used for pre-treatment with lipopolysaccharide (LPS) and then incubated with **Mi-OCl-RP**. Compared with untreated cells (Fig. 6 **1a-1c**), the fluorescence intensity of the green signal was significantly increased, and the red signal was significantly decreased in the LPS-treated RAW 264.7 (Fig. 6 **2a-2c**). Subsequently, treatment of LPS caused an increased level of endogenous OCl^-, which resulted in the elevated fluorescence signal, as apparently visualized by imaging. As shown in Fig. 6 **4a-4c**, the cells were incubated with LPS and when 4-aminobenzoic acid hydrazide (ABAH, which is a specific inhibitor of MPO that suppressed the generation of HOCl) is added, the fluorescence signal was approximately the same as that

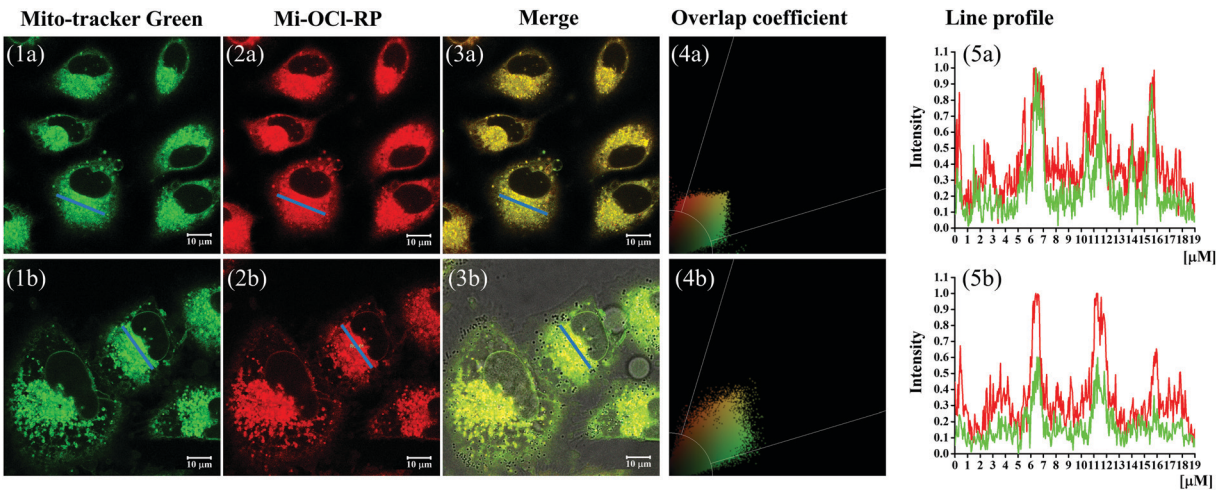

Fig. 5 Confocal fluorescence images of A549 cells pre-stained with **Mi-OCl-RP** and subsequently co-incubated with Mito Tracker Green. (**1a**, **1b**) Images of Mito Tracker Green (λ_{ex} = 490 nm, λ_{em} = 500–550 nm); (**2a**) images of **Mi-OCl-RP** (λ_{ex} = 405 nm, λ_{em} = 420–520 nm); (**2b**) images of **Mi-OCl-RP** (λ_{ex} = 588 nm, λ_{em} = 600–700 nm); (**3a**) merge of **1a** and **2a**; (**3b**) merge of **1b** and **2b**; (**4a**) the overlap coefficients of excitation at 490 and 405 nm; (**4b**) the overlap coefficients of excitation at 490 and 588 nm; (**5a**, **5b**) the intensity profile of the ROI in merge images. Scar bar: 10 μm.

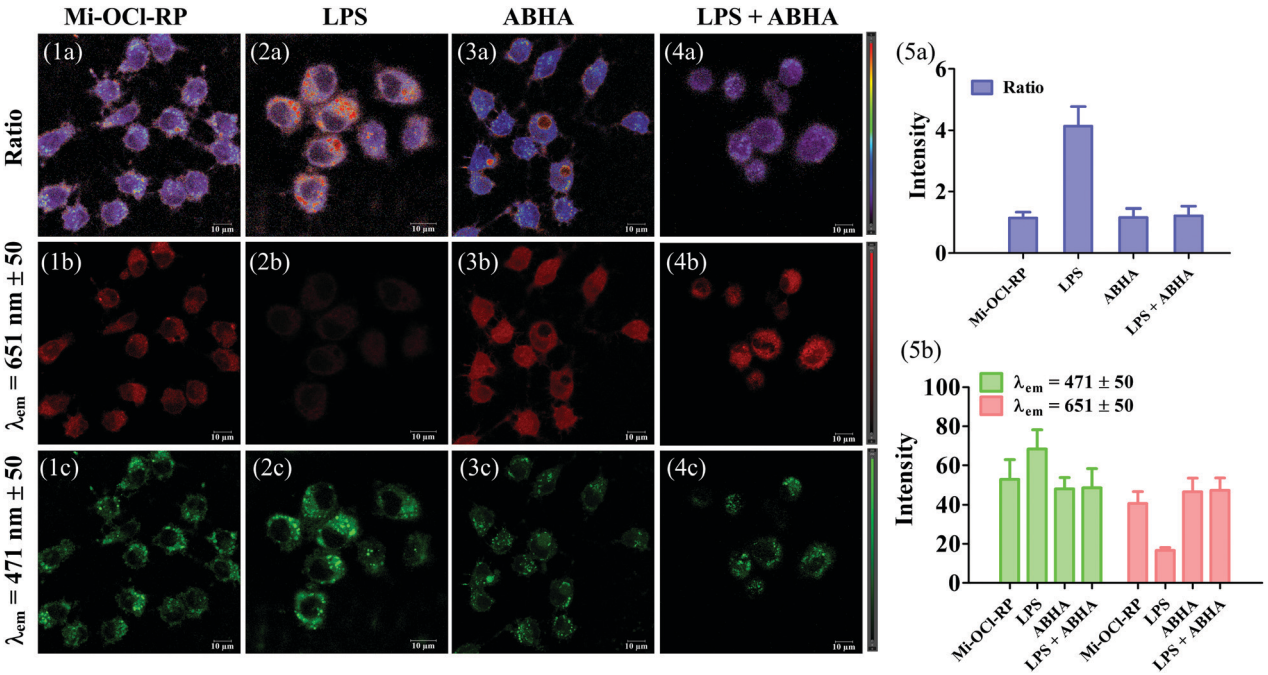

Fig. 6 Confocal fluorescence images of **Mi-OCl-RP** responding to endogenous OCl^- in RAW264.7 cells. (**1a-1c**) Macrophages treated with **Mi-OCl-RP** (10 μM) for 20 min; (**2a-2c**) macrophages pretreated with LPS (1.0 μg mL^{-1}) for 3 h after preincubation with **Mi-OCl-RP** (10 μM) for another 20 min; (**3a-3c**) macrophages pretreated with 200.0 μM ABAH for 60 min after preincubation with **Mi-OCl-RP** (10 μM) for another 20 min; (**4a-4c**) macrophages pretreated with LPS (1.0 μg mL^{-1}) for another 3 h after stimulation with 200.0 μM ABAH for 60 min, and then incubated with **Mi-OCl-RP** (10 μM) for 20 min (**1a-4b**, ratio of two emission images; **1a-4b**, λ_{ex} = 588 nm, λ_{em} = 600–700 nm; **1c-4c**, λ_{ex} = 405 nm, λ_{em} = 420–520 nm); (**5a**, **5b**) Quantified relative fluorescence intensity of images. Scar bar: 10 μm.

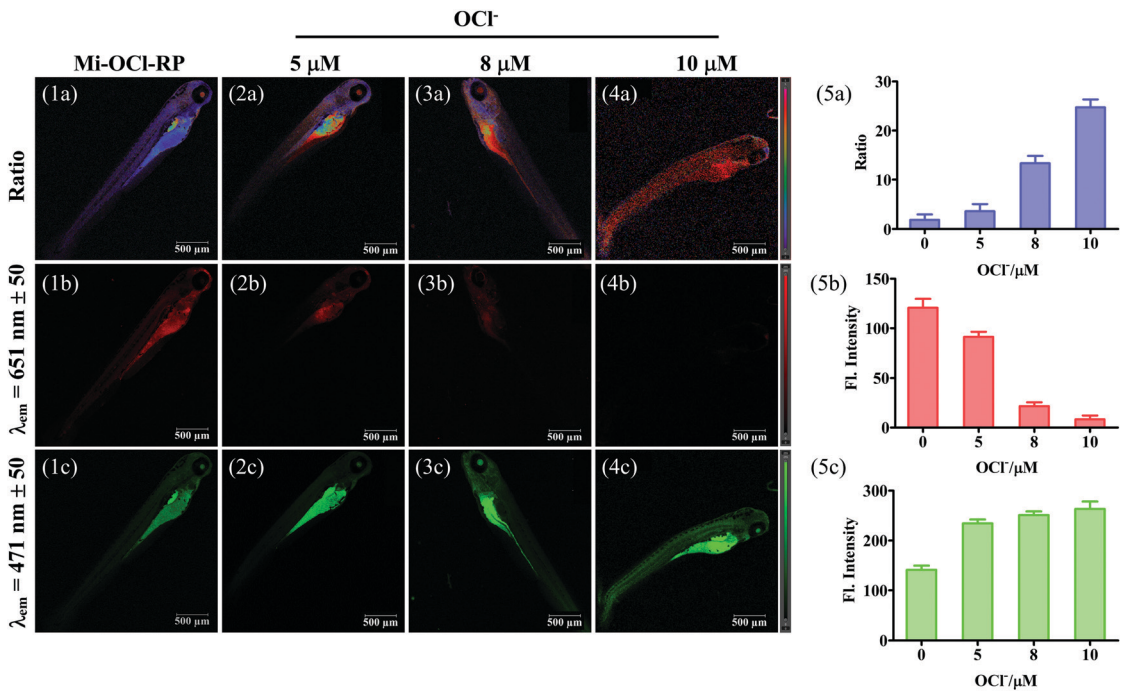

Fig. 7 Confocal fluorescence images of **Mi-OCl-RP** responding to OCl^- in zebrafish. (**1a-1c**) Zebrafish incubated with **Mi-OCl-RP** (10 μM, 30 min); (**2a-4c**) Zebrafish incubated with OCl^- (5, 8 and 10 μM) for 10 min and then incubated with **Mi-OCl-RP** (10 μM, 30 min). First column: images of ratios of excitation at 405 and 588 nm; second column: excitation at 588 nm; third column: excitation at 405 nm. (**5a-5c**) Quantified relative fluorescence intensity of images **1a-4c**. Scale bar: 500 μm.

of the signal of the control group (the cells were stained with the ABHA scavenger or the pure probe, Fig. 6 **3a-3c**). The quantitative analysis results showed that the fluorescence intensity after treatment with LPS enhanced compared to that of the untreated cells (Fig. 6 **5a-5b**). These findings support that **Mi-OCl-RP** is competent for imaging endogenous OCl^- at the cellular level.

Ratiometric fluorescence imaging of OCl^- in zebrafish

According to the preliminary imaging studies in living cells, we further investigate the efficacy of **Mi-OCl-RP** monitoring OCl^- in zebrafish. As shown in Fig. 7 **1a-1c**, the zebrafish were incubated with only **Mi-OCl-RP** (10 μM), which showed bright green and red fluorescence signals. After the treatment with 5 μM or 8 μM OCl^- for 10 min, the green fluorescence was significantly enhanced, and dim red fluorescence was obtained at the same time (Fig. 7 **2a-3c**). At the same time, when zebrafish were treated with a higher concentration of OCl^- (10 μM), the green fluorescence relatively strengthened, and the red fluorescence faded (Fig. 7 **4a-4c**). It can be seen that the green fluorescence intensity was gradually increased and the red fluorescence intensity was evidently decreased. Similarly, the ratios of fluorescence intensity (F_{green}/F_{red}) showed enhancement (Fig. 7 **5a-5c**). The ratiometric fluorescence of zebrafish imaging is also consistent with the results of living cells imaging. The results indicate that **Mi-OCl-RP** is applicable in detecting OCl^- *in vivo*, effectively.

Conclusion

In summary, a novel mitochondria-targeted ratiometric fluorescent probe **Mi-OCl-RP** was successfully engineered. Molecular docking calculation indicated that ANT could be the potential molecular target of **Mi-OCl-RP**. The high binding energy (-8.58 kcal mol^{-1}) may explain the high mitochondria selectivity of **Mi-OCl-RP**. The new probe possesses highly favorable properties, including ratiometric fluorescence response signals to OCl^- (within 7 s), high selectivity and sensitivity, and a large Stokes shift (278 nm), which could be easily observed by the naked eye. In addition, the colocalization coefficient suggested that **Mi-OCl-RP** can effectively target mitochondria. Moreover, **Mi-OCl-RP** has good permeability and low toxicity, and was effectively employed in real-time and ratiometric imaging of OCl^- *in vivo*. We expect that the probe could have great effect on the study of mitochondria-targeted protein and biological functions of OCl^- in the living system.

Conflicts of interest

There are no conflicts to declare.

Acknowledgements

This work was financially supported by the National Natural Science Foundation of China (21672083, 21877048, and 22077048), and the startup fund of Guangxi University (A3040051003).

Notes and references

1 P. M. Quiros, A. Mottis and J. Auwerx, *Nat. Rev. Mol. Cell Biol.*, 2016, **17**, 213–226.
2 H. Cho, Y. Cho, M. S. Shim, J. Y. Lee, H. S. Lee and H. Kang, *BBA, Mol. Basis Dis.*, 2020, **1866**, 165808.
3 B. Zhivotovsky, L. Galluzzi, O. Kepp and G. Kroemer, *Cell Death Differ.*, 2009, **16**, 1419–1425.
4 J. I. Park, S. G. Kim, M. W. Beak, T. J. Park, I. K. Lim, Y. M. Seo and S. Y. Chun, *Mol. Cell. Endocrinol.*, 2013, **367**, 31–40.
5 C. P. Baines and J. D. Molkentin, *J. Mol. Cell. Cardiol.*, 2009, **46**, 969–977.
6 T. Finkel and N. J. Holbrook, *Nature*, 2000, **408**, 239–247.
7 C. C. Winterbourn, *Nat. Chem. Biol.*, 2008, **4**, 278–286.
8 Z. Lou, P. Li and K. Han, *Acc. Chem. Res.*, 2015, **48**, 1358–1368.
9 (*a*) X. Chen, X. Tian, I. Shin and J. Yoon, *Chem. Soc. Rev.*, 2011, **40**, 4783–4804; (*b*) K. M. Holmström and T. Finkel, *Nat. Rev. Mol. Cell Biol.*, 2014, **15**, 411–421.
10 M. P. Murphy, A. Holmgren, N. G. Larsson, B. Halliwell, C. J. Chang, B. Kalyanaraman, S. G. Rhee, P. J. Thornalley, L. D. Partridge, T. Gems Nystrom, V. V. Belousov, P. T. Schumacker and C. C. Winterbourn, *Cell Metab.*, 2011, **13**, 361–366.
11 (*a*) Z. M. Prokopowicz, F. Arce, R. Biedron, C. L.-L. Chiang, M. Ciszek, D. R. Katz, M. Nowakowska, S. Zapotoczny, J. Marcinkiewicz and B. M. Chain, *J. Immunol.*, 2010, **184**, 824–835; (*b*) Y. Koide, Y. Urano, K. Hanaoka, T. Terai and T. Nagano, *J. Am. Chem. Soc.*, 2011, **133**, 5680–5682.
12 B. M. Fournier and C. A. Parkos, *Mucosal Immunol.*, 2012, **5**, 354–366.
13 N. Branzk, A. Lubojemska, S. E. Hardison, Q. Wang, M. G. Gutierrez, G. D. Brown and V. Papayannopoulos, *Nat. Immunol.*, 2014, **15**, 1017–1025.
14 Y. W. Yap, M. Whiteman and N. S. Cheung, *Cell. Signalling*, 2007, **19**, 219–228.
15 R. Zhang, B. Song and J. Yuan, *TrAC, Trends Anal. Chem.*, 2018, **99**, 1–33.
16 S. Hammerschmidt, N. Buchler and H. Wahn, *Chest*, 2002, **121**, 573–581.
17 X. Chen, X. Tian, I. Shin and J. Yoon, *Chem. Soc. Rev.*, 2011, **40**, 4783–4804.
18 U. Forstermann, N. Xia and H. Li, *Circ. Res.*, 2017, **120**, 713–735.
19 S. Sugiyama, K. Kugiyama, M. Aikawa, S. Nakamura, H. Ogawa and P. Libby, *Arterioscler., Thromb., Vasc. Biol.*, 2004, **24**, 1309–1314.
20 Y. Chen, C. Zhu, J. Cen, Y. Bai, W. He and Z. Guo, *Chem. Sci.*, 2015, **6**, 3187–3194.
21 J. Santo-Domingo and N. Demaurex, *J. Gen. Physiol.*, 2012, **139**, 415–423.
22 J. Han and K. Burgess, *Chem. Rev.*, 2010, **110**, 2709–2728.
23 T. D. Ashton, K. A. Jolliffe and F. M. Pefeffer, *Chem. Soc. Rev.*, 2015, **44**, 4547–4595.
24 C. Duan, M. Won, P. Verwilst, J. Xu, H. S. Kim, L. Zeng and J. S. Kim, *Anal. Chem.*, 2019, **91**, 4172–4178.
25 Q. Hu, C. Qin, L. Huang, H. Wang, Q. Liu and L. Zeng, *Dyes Pigm.*, 2018, **149**, 253–260.

26 L. Zeng, T. Chen, B. Chen, H. Yuan, R. Sheng and G. Bao, *J. Mater. Chem. B*, 2020, **8**, 1914–1921.
27 L. Yuan, W. Lin, K. Zheng, L. He and W. Huang, *Chem. Soc. Rev.*, 2013, **42**, 622–661.
28 Z. Q. Guo, S. Park, J. Yoon and I. Shin, *Chem. Soc. Rev.*, 2014, **43**, 16–29.
29 H. Li, G. X. Zhang, H. M. Ma, D. Q. Zhang, J. Li and D. B. Zhu, *J. Am. Chem. Soc.*, 2004, **126**, 11543–11548.
30 L. Yuan, W. Lin, Y. Yang and H. Chen, *J. Am. Chem. Soc.*, 2012, **134**, 1200–1211.
31 Q. Xu, C. H. Heo, J. A. Kim, H. S. Lee, Y. Hu, D. Kim, K. M. K. Swamy, G. Kim, S.-J. Nam, H. M. Kim and J. Yoon, *Anal. Chem.*, 2016, **88**, 6615–6620.
32 P. H. P. R. Carvalho, J. R. Correa, B. C. Guido, C. C. Gatto, H. C. B. De Oliveira, T. A. Soares and B. A. D. Neto, *Chem. – Eur. J.*, 2014, **20**, 15360–15374.
33 E. Pebay-Peyroula, C. Dahout-Gonzalez, R. Kahn, V. Trezeguet, G. J. M. Lauquin and R. Brandolin, *Nature*, 2003, **426**, 39–41.
34 L. Pu, *Chem. Rev.*, 2004, **104**, 1687.